Article

Particle Cut Diameter Prediction of Uniflow Cyclone Systems with Fuzzy System Analysis

Vinzenz Klapper [1,*], **Giovanni Luzi** [1], **Benedict Prah** [1] **and Antonio Delgado** [2]

1   German Research and Development Center, LSTME Busan, 1276 Jisa-Dong, Busan 46742, Republic of Korea; giovanni.luzi@lstme.org (G.L.)
2   Faculty of Engineering, Institute of Fluid Mechanics (LSTM), Friedrich-Alexander-University Erlangen-Nuremberg (FAU), Cauerstraße 4, 91058 Erlangen, Germany; antonio.delgado@fau.de
*   Correspondence: vinzenz.klapper@lstme.org

Abstract: Cyclones are devices used in various industries to remove particulate matter from gases and liquids. Commonly used in the power generation, cement, and mining industries, cyclones improve the efficiency and longevity of equipment by removing dust and other small particles that can cause wear and damage. Among centrifugal separation, reverse-flow cyclones are primarily used for particle separation, which can reach heights of several meters on an industrial scale and therefore, are difficult to access for maintenance. A uniflow centrifugal segregation system avoids these drawbacks of reverse-flow cyclones since their accessibility is good and their height usually does not exceed their diameter. The efficiency is a critical aspect of separating systems. This study systematically examines the collection efficiency for particles ranging from $1\,\mu m$ to $29\,\mu m$ in diameter based on varying vane angles of the swirl inducer at flow rates ranging from $130\,L\,s^{-1}$ to $236\,L\,s^{-1}$.

Keywords: uniflow cyclone; particle separation; particle cut diameter; fractional particle separation efficiency; prediction model; fuzzy logic

1. Introduction

Most emerging economies and industrialized nations are facing problems with fine dust pollution. In South Korea, extremely high fine and ultra-fine dust levels are experienced every winter and through out the spring [1]. Dust separators help to reduce the environmental impact of industrial operations by preventing the release of dust and other particles into the atmosphere [2,3]. The primary sources of fine and ultra-fine dust within the ambient air are fossil fuel combustion products [4] and road traffic effects such as tire and brake wear and suspension of road dust, especially under dry weather conditions [2,5]. Other natural sources, like dust storms, contribute to a higher fine dust concentration. To reduce the fine dust contamination of the environment and indoor contamination, fine dust must be collected before the release into the ambient air, which requires enclosed indoor air to be cleaned of the dust particle. Dust is classified scientifically according to particle size. Coarse particulate matter is defined as having a diameter d_p between $2.5\,\mu m$ and $10\,\mu m$ [6]. While the fine particulate matter is defined as having a diameter smaller than $2.5\,\mu m$, its size exhibits a significant health hazard. Further, ultra-fine dust is classified being smaller than $0.1\,\mu m$. As a result, fine dust and ultra-fine dust contribute to various illnesses and health problems, including lung cancer, bronchial asthma, cardiovascular and cerebrovascular diseases, pulmonary mortality, arteriosclerosis, coronary heart disease, and early death [7].

Centrifugal separators, also called cyclones, collect fine and ultra-fine dust and are distinguished into two groups. First reverse-flow cyclones, most commonly known, have been widely researched during the last half of the previous century. Many tests with reverse-flow cyclones concerning the dependency of the efficiency from setup parameters have been conducted. Lapple and Stairmand [3] set the foundation of cyclone research in the 1950s.

During their observations a particle cut diameter d_{pc} of 1.38 µm was achieved [8]. Dirgo [8] and Iozia [9], used vapor from mineral oil using a Laskin-Nozzle setup to generate aerosol particles. Unlike fine powders or dust, mineral oil droplets forms ideal sphere-shaped aerosol particles that do not re-entrain or rebound toward the cyclone wall. Furthermore, mineral oil droplets tend to agglomerate and deliver therefore commonly a better result in terms of particle cut diameter d_{pc} and cyclone efficiency η. On the other hand, mineral oils can clog sensors or cover lenses from optical measurement devices, such as particle size analyzers and filters. Due to the solid nature of fine and ultra-fine dust particles, which can have different chemical compositions, they are rinsed off easily with water or ethanol from experimental setups while cleaning the system. Therefore fine and ultra-fine dust used as test dust exhibits benefits. In uniflow cyclone systems, the particle-laden flow does not change the flow direction, as is the case for reverse-flow cyclones. The main flow direction is parallel to the cyclone axis, and a swirl inducer or tangential inlet introduces the rotational motion of the gas. In this way, turbulence and pressure drop can be reduced [10]. Since the pressure drop of a cyclone system is proportional to the energy required for guiding contaminated gases through the cyclone, reducing the pressure drop of a cyclone is essential to design a highly efficient system. The particle cut diameter is a measure of the efficiency of a cyclone system. It is defined as the particle size of which 50% are separated, while 50% of the particles exit the separation system. Predicting the particle cut diameter in dependence on experimental data, reduces the total time of measurements necessary and supports the adjustment of the process parameter. Fuzzy logic system analysis, as part of machine learning [11], is an established method to build a predictive tool. It is a theory developed in the 1965s by Lotfi Zadeh, a professor at UC Berkeley. Unlike binary logic, fuzzy logic is variable-valued logic, where the degree of truth can represent any number between 0 and 1. Many applications in daily life use fuzzy logic, such as washing machines, air-conditioning systems, and subways [12]. Other examples are sheet rolling control in food processing [13], prediction of rainfall in particular regions using weather data [14], or surface roughness prediction based on milling machines parameters [11]. Fuzzy logic is used for process controlling and prediction based on limited amounts of data, which makes it an valuable method for predicting parameters. The aim of this work is to proof the excellent separation capabilities of uniflow cyclones in comparison with reverse-flow cyclones and to develop a prediction tool based on the experimental data using a fuzzy logic approach.

2. Materials and Methods

2.1. Experimental Setup and Velocity Measurements

For the experimental measurements an uniflow cyclone system, consisting of a particle feeder, an axial blower, a separating chamber and a highly efficient particulate air filter (HEPA)-filter is set up. An axial rotating gas behind the blower (GBL80320, Greenworks©, Changzhou, China) [15] is further amplified in its rotating motion by swirl inducers with different vane angles β_v. Each of the five swirl inducers are designed with four curved vanes that guide the air into the system (Figure 1). A diffuser connects the swirl inducer section point A (Figure 2) with the separation chamber. The separation chamber consists of a poly-acrylic tube (wall thickness = 5 mm, inner diameter = 150 mm, length = 1000 mm). The flow is guided though the separation chamber into a hollow conical-shaped outlet duct point B (Figure 2), which consists of a FDM-printed annular cone connected with a poly-acrylic tube (wall thickness = 2 mm, inner diameter = 86 mm, length = 500 mm).
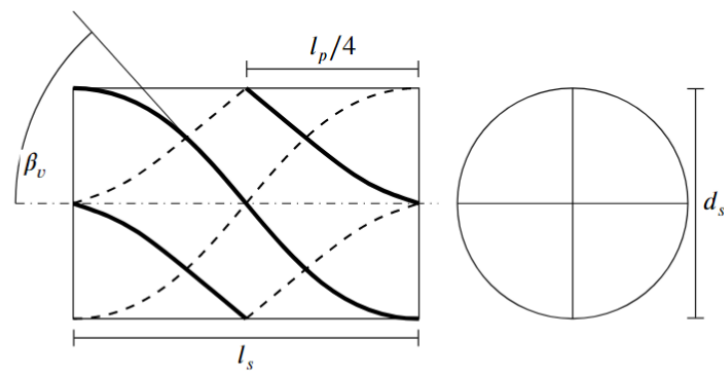
Figure 1. General swirl inducer dimensions.

Inside the outlet tube, a multi-channel structure (length = 50 mm, channel diameter = 5 mm) is installed as a flow straightener, which reduces the rotation of the flow and conditions the air stream for distribution measurement with a particle spectrometer (Promo 2000, PALAS GmbH, Karlsruhe Germany). To prevent fine and ultra-fine dust particles from leaving the experimental setup and entering the environment, a HEPA-filter (SC-FIS-CT 26, Festool GmbH, Wendlingen, Germany) seals the end of the outlet tube.
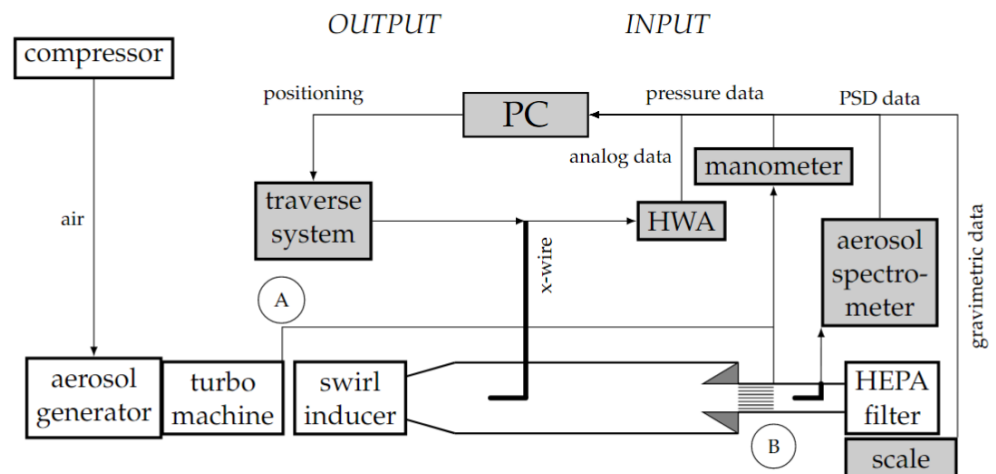
Figure 2. Schematic diagram of the experimental setup.

The geometric parameters that characterize the swirl inducers, namely vane angle β_v, twist ratio $\frac{l}{d}$, pitch length l_p and geometrical swirl number S_g are given in Table 1. Labels are given with VA0 to VA60 based on the value of the vane angle β_v of the swirl inducer. The geometrical swirl number S_g is calculated as

$$S_g = \frac{2}{3}\left(\frac{1 - \left(d_{hub}/d_{in}\right)^3}{1 - \left(d_{hub}/d_s\right)^2}\right)\tan(\beta_v),\tag{1}$$

following Litvinov [16]. Where d_i is the diameter of the inlet, d_s is the swirl tape diameter, d_{hub} is the diameter of the hub, and β_v is the vane angle of the swirl inducer. A vane angle β_v of 0° named as VA0, is used as a label for the setup without a swirl inducer. Each swirl inducer is separately placed between the axial turbo machine and the diffuser , connecting the separation chamber.

Table 1. Overview of the examined swirl inducers.

	Symbol	Unit	VA0	VA20	VA30	VA40	VA50	VA60
length	l_s	mm	0	112.5	67.5	45	67.5	45
diameter	d_s	mm	0	77	77	77	77	77
vane angle	β_v	°	0	18.9	29.7	40.5	48.8	59.7
twist ratio	$\frac{l}{d}$	-	-	1.46	0.88	0.58	0.88	0.58
pitch length	l_p	mm	-	450	270	180	135	90
geom. swirl nb	S_g	-	-	0.23	0.38	0.57	0.76	1.14

Prior to the fractional distribution measurements inside the outlet of the uniflow cyclone, the velocities at the entrance of the separation chamber are measured along the diameter of the tube with a Hot-Wire-Anemometer (Dantec Dynamic A/S, Skovlunde, Denmark) to quantify the intensity of rotation caused by each swirl inducer. The velocity measurements are conducted using an L-shaped probe holder fitted with an X-probe. The X-probe is positioned 250 mm from the swirl inducer and is guided into the separation chamber through a slot in the tube.

During the separation investigations, 18 setup configurations are examined, and the fractional separation efficiency is analyzed. While six different swirl inducer settings are applied, the volumetric flow rate $\dot{V}$ is changed in three steps between $0.130 \, \text{m}^3 \, \text{s}^{-1}$ to $0.236 \, \text{m}^3 \, \text{s}^{-1}$. The Reynolds number R_c is calculated as

$$Re_c = \frac{v_{in} \cdot d}{\nu} \tag{2}$$

using the mean axial velocity of the fluid v_i at the entrance of the separation chamber of the cyclone, ν as the kinematic viscosity of the fluid and d_i the diameter of the inlet [17]. The particle size distribution of the ultra-fine test dust (A1—Arizona test dust, Powder Technology Inc.©(PTI), Arden Hills, MN, USA), with a bulk density of $\rho_b = 500 \, \text{kg} \, \text{m}^{-3}$ and a particle density of $\rho_p = 2650 \, \text{kg} \, \text{m}^{-3}$, is initially analyzed with a light-scattering aerosol spectrometer. The analysis of the test dust provided a mean particle size distribution in a particle size range of 0.5 μm to 40 μm, which matches the information in the data sheet provided by the supplier.

An aerosol generator with a rotating brush distributes the fine particles into the air stream. The brush transports the particulate matter from the reservoir of the aerosol generator into a pre-loaded air stream before it is released into the inlet of the turbo machine.

Next, the particle-laden gas undergoes a diffuser-controlled expansion, significantly reducing its velocity. The rotating motion caused by the swirl inducer originates centrifugal forces on the gas and particles within and further leads to a trajectory of the fine dust particles towards the cyclone wall. In the particle theory, these particles have a stokes number of $Stk \gg 1$ [18]. For the simplicity of the design and a stable rotating flow, the separated particles are collected in the annular space between the cyclone and the conical outlet. This is possible due to the low particle load. Fine dust particles with a stokes number of $Stk \ll 1$ remain within the gas flow and leave the separation chamber until finally collected inside the HEPA-filter. The pressure drop Δp is measured over the cyclone between Point A and B shown in Figure 2, specifically over the inlet, the diffuser, the separation chamber, and the outlet, using a digital differential pressure sensor (SDP 810, Sensirion AG, Stäfa, Switzerland) with a bidirectional pressure range of $\Delta p = \pm 600 \, \text{Pa}$. The two pitot tubes used for the pressure drop measurement are placed in the center of the inlet and outlet tubes along the cyclone axis. Straightening fins behind the axial blower inside the inlet tube and the flow straightener inside the outlet tube are conditioning the flow for a correct pressure measurement. The recording is conducted with a sampling rate of 10 ms and a measurement period of 10 s.

2.2. Particle Separation Efficiency Measurements

Prior to the particle distribution measurements at the outlet of the uniflow cyclone, several pre-trials were performed to charge the cyclone walls with fine dust particles in order to minimize electro-static effects between cyclone wall and fine particles during the measurements. To calculate the separation efficiency and the particle cut diameter d_{pc} of each of the swirl inducer configurations for the respective flow velocities, three measurements for each of the 18 process parameter settings are performed. Prior to and after each measurement, the weight of the fine test dust in the aerosol generator, and the weight of the HEPA-filter is determined to calculate the total weight of the fine dust particle m_{in} entering the system and the total weight of the particles m_f that are leaving the system during the experiment and remain in the HEPA-filter. The fine dust powder injection, using an aerosol generator at the cyclone inlet, was performed at an average concentration of $c_i = 16.2\,\mathrm{mg\,m^{-3}}$. The particle spectrometer analyzes the particle size distribution of the air stream entering the filter media during each trial for 120 s. With the known particle size distributions f_{in} of the fine dust (compare Figure 3) and the distribution of the particles that are leaving the uniflow cyclone f_{out}, the fractional separation efficiency of a given particle size range is calculated using Equation (3) given by Faulkner [19]

$$\eta_i = \frac{m_{in} \cdot f_{in,i} - m_f \cdot f_{out,i}}{m_{in} \cdot f_{in,i}}. \tag{3}$$

The fractional separation efficiencies calculated are displayed as a fractional separation efficiency curve, where the particle cut diameter d_{pc} is calculated using an approximated logistic function proposed by Iozia and Leith [9]. The approximation of the logistic curve and the visualization of the data were conducted using Python.
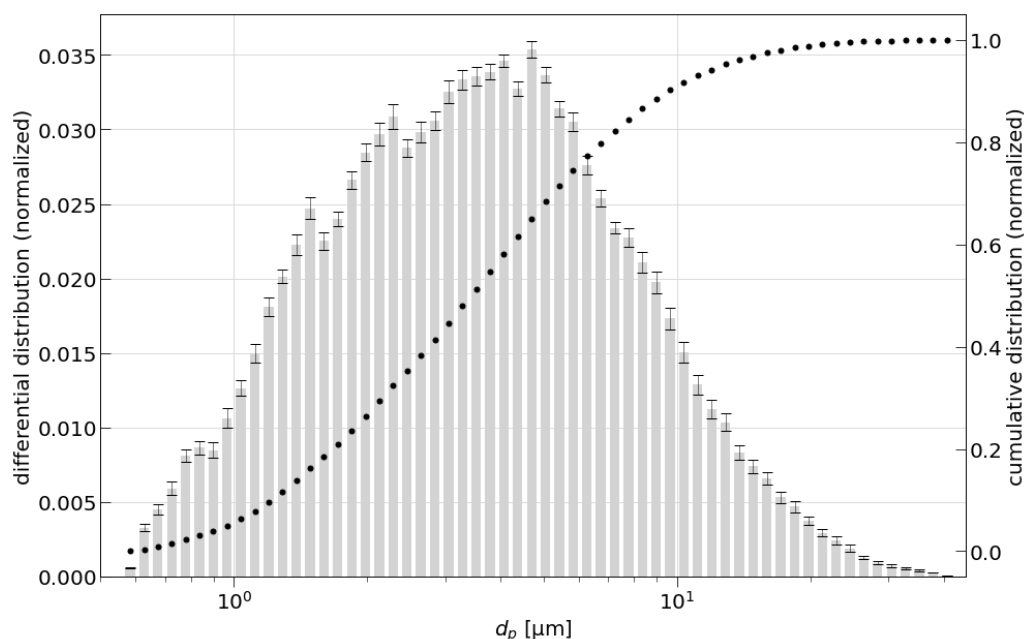
Figure 3. Differential and cumulative particle size distribution of the used fine test dust.

2.3. Fuzzy Logic Prediction Model

In the fuzzy logic theory, knowledge is interpreted as a collection of elastic or equivalent fuzzy constraints on a collection of variables [20]. Compared to a crisp or binary set with clear boundaries, a fuzzy set is described in grades [21]. In a fuzzy set, close values have similar grades of membership and are therefore less prone to errors. More advantages of fuzzy logic models compared to other predictive models such as machine learning predictive models, are the clearness of the structure and that it is feasible also when

the amount of data is scarce. In the case of the experimental data, the input parameters for a fuzzy system is represented by the pressure drop Δp and the respective vane angle β_v of the swirl inducer, which is described in a fuzzy set. The particle cut diameter d_{pc} is a measure for the overall efficiency of the cyclonic system in relation with a specific particle size d_p. Consequently the particle cut diameter d_{pc} will be the output variable of the proposed fuzzy system (Figure 4).
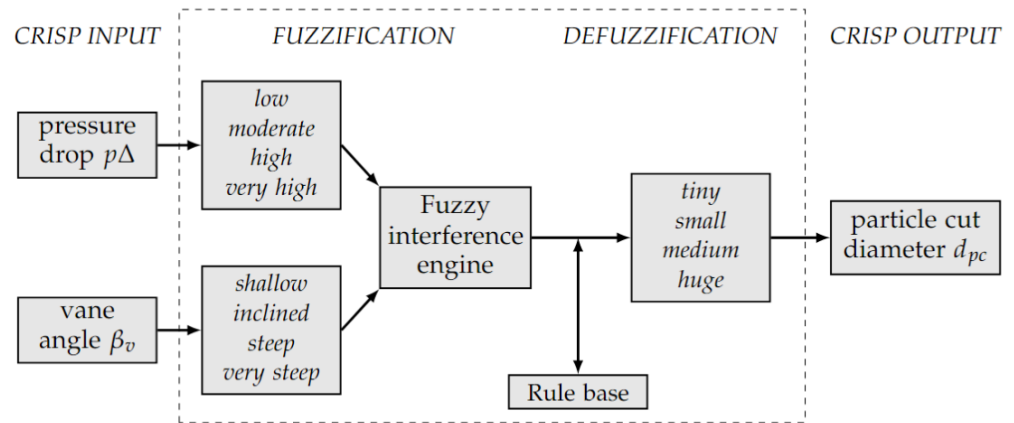
Figure 4. Schematic diagram of the fuzzy logic model.

In a fuzzy logic model the accuracy of the prediction is proportional to the number of the parametric domains represented by the membership functions. With an increasing number of membership functions, the complexity of the model increases. Figure 5 displays the results from the experimental investigations on the uniflow cyclone. The resulting particle cut diameter d_{pc} are annotated next to the markers. It can be seen that the the pressure drop Δp is a non-independent variable, which increases while the vane angle β_v increases. Since the pressure drop Δp is not solely depending on the vane angle β_v, but as well on other variables such as flow velocity v_i, geometric variables of the cyclone, surface roughness, to name a few, the pressure drop Δp is applicable as an input variable for fuzzy logic prediction.
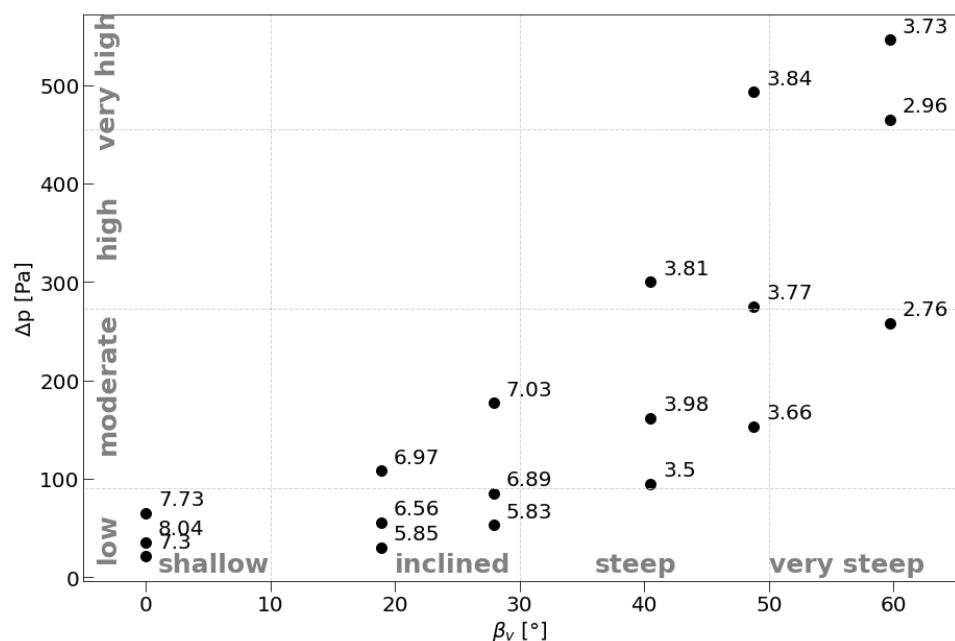
Figure 5. The particle cut diameter d_{pc} as a result of pressure drop Δp and the vane angle β_v with the domain of the linguistic terms.

The range of the measured pressure drop values Δp is categorized into four linguistic terms, called pressure domains, which are namely low, moderate, high, and very high pressure drop. Further, the range of the examined vane angle β_v of the swirl inducers is classified into four designated domains as well: shallow, inclined, steep, and very steep. The exact range of the domains is listed in Table 2.

Table 2. Linguistic terms of the fuzzy sets and their respective ranges

Parameter	Linguistic Term	Abbreviation	Range	Unit
pressure drop Δp	low	l	0–91	Pa
	moderate	m	91–273	Pa
	high	h	273–455	Pa
	very high	vh	455–546	Pa
vane angle β_v	shallow	sh	0–10	°
	inclined	i	10–30	°
	steep	st	30–50	°
	very steep	vs	50–60	°
particle cut diameter d_{pc}	tiny	t	2.76–3.64	μm
	small	s	3.64–5.40	μm
	medium	m	5.40–7.16	μm
	huge	h	7.16–8.04	μm

2.3.1. Membership Functions and Fuzzification

Membership functions describe the degree of membership or value of truth of a specific fuzzy input parameter and are either discrete or continuous. Being numerical representations of the linguistic concepts, membership functions can be built either through learning from data or experts' opinion [12]. Describing a membership function, U is called the universe, and μ_x is a fuzzy set of U. In the case of the fuzzy set for the pressure drop $\mu(p\Delta)$ and the fuzzy set for the vane angle $\mu(\beta_v)$ as well as the fuzzy set particle cut diameter $\mu(d_{pc})$, triangular membership functions are used. The following fuzzy sets consist of one open-left, two closed, and one open-right membership function. The membership functions (Figure 6) of the fuzzy set $\mu(p\Delta)$ are $\mu_l(p\Delta)$, $\mu_m(p\Delta)$, $\mu_h(p\Delta)$ and $\mu_{vh}(p\Delta)$ represent the fuzzy set as

$$\mu(p\Delta) = \mu_l(p\Delta) + \mu_m(p\Delta) + \mu_h(p\Delta) + \mu_{vh}(p\Delta) = 1 \quad p\Delta \in U. \tag{4}$$
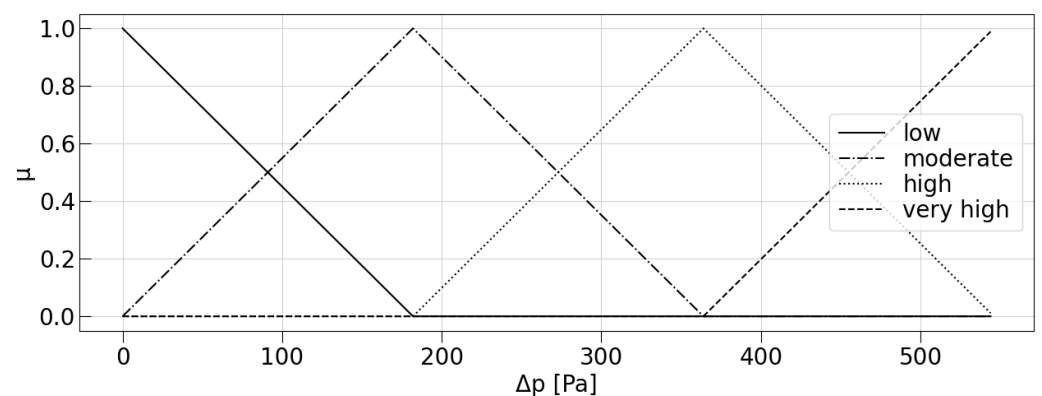
Figure 6. Membership functions of the pressure drop Δp.

The pressure is described by a certain degree of membership from the membership function, commonly referred to as fuzzification.

$$
\mu_l(p\Delta) = \begin{cases} 0 & for \quad p\Delta \leq 0 \\ \frac{182-p\Delta}{182} & for \quad 0 \leq p\Delta \leq 182 \\ 0 & for \quad 182 \leq p\Delta \end{cases} \tag{5}
$$

$$
\mu_m(p\Delta) = \begin{cases} 0 & for \quad p\Delta \leq 0 \\ \frac{p\Delta}{182} & for \quad 0 \leq p\Delta \leq 182 \\ \frac{364-p\Delta}{182} & for \quad 182 \leq p\Delta \leq 364 \\ 0 & for \quad 364 \leq p\Delta \end{cases} \tag{6}
$$

$$
\mu_h(p\Delta) = \begin{cases} 0 & for \quad p\Delta \leq 182 \\ \frac{p\Delta-182}{182} & for \quad 182 \leq p\Delta \leq 364 \\ \frac{546-p\Delta}{182} & for \quad 364 \leq p\Delta \leq 546 \\ 0 & for \quad 546 \leq p\Delta \end{cases} \tag{7}
$$

$$
\mu_{vh}(p\Delta) = \begin{cases} 0 & for \quad p\Delta \leq 364 \\ \frac{p\Delta-364}{182} & for \quad 364 \leq p\Delta \leq 546 \\ 0 & for \quad 546 \leq p\Delta. \end{cases} \tag{8}
$$

Similarly the fuzzy set $\mu(\beta_v)$, which represents the vane angle β_v, is defined. The membership functions (Figure 7) of the fuzzy set $\mu(\beta_v)$ are $\mu_s(\beta_v)$, $\mu_i(\beta_v)$, $\mu_s(\beta_v)$ and $\mu_{vs}(\beta_v)$ represent the fuzzy set in the universe V as

$$
\mu(\beta_v) = \mu_{sh}(\beta_v) + \mu_i(\beta_v) + \mu_{st}(\beta_v) + \mu_{vs}(\beta_v) = 1 \quad \beta_v \in V. \tag{9}
$$
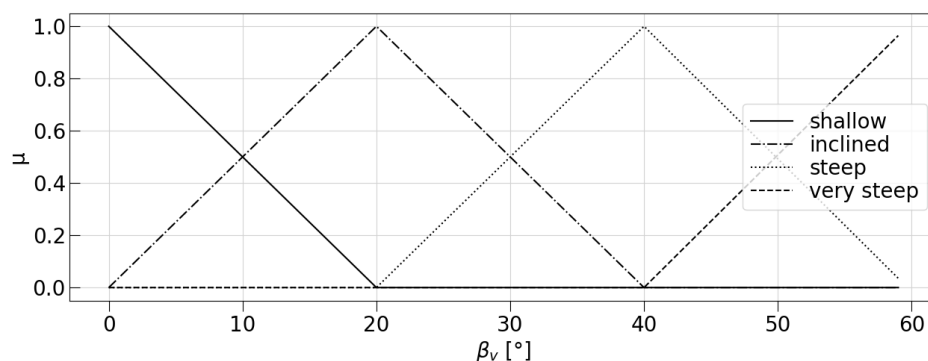
Figure 7. Membership functions of the vane angle β_v.

With the use of the membership functions the degree of membership can be calculated as

$$
\mu_{sh}(\beta_v) = \begin{cases} 0 & for \quad \beta_v \leq 0 \\ \frac{20-\beta}{20} & for \quad 0 \leq \beta_v \leq 20 \\ 0 & for \quad 20 \leq \beta_v \end{cases} \tag{10}
$$

$$
\mu_i(\beta_v) = \begin{cases} 0 & for \quad \beta_v \leq 0 \\ \frac{\beta_v}{20} & for \quad 0 \leq \beta_v \leq 20 \\ \frac{40-\beta_v}{20} & for \quad 20 \leq \beta_v \leq 40 \\ 0 & for \quad 40 \leq \beta_v \end{cases} \tag{11}
$$

$$\mu_{st}(\beta_v) = \begin{cases} 0 & for & \beta_v \leq 20 \\ \frac{\beta_v - 20}{20} & for & 20 \leq \beta_v \leq 40 \\ \frac{60 - \beta_v}{20} & for & 40 \leq \beta_v \leq 60 \\ 0 & for & 60 \leq \beta_v \end{cases} \tag{12}$$

$$\mu_{vs}(\beta_v) = \begin{cases} 0 & for & \beta_v \leq 40 \\ \frac{\beta_v - 40}{20} & for & 40 \leq \beta_v \leq 60 \\ 0 & for & 60 \leq \beta_v. \end{cases} \tag{13}$$

2.3.2. Fuzzy Operators and Fuzzy Rules

The maximum possible rules of a fuzzy system depend on the number of input parameters and the number of linguistic terms used. As a matter of fact the number of rules do not exceed the number of linguistic terms to the power of input parameters chosen [12]. Therefore, a maximum number of sixteen fuzzy rules can be created with two input parameters and four linguistic terms each. On the other hand, not all rules must be formulated to achieve high prediction accuracy. Based on the experimental results in Figure 5, the rules are generated in connection to the defined domains. Since some domains are empty, the maximum number of rules can not be achieved (cp. Figure 5). For the empty domains, no data points have been recorded. Therefore no information can be retrieved from these domains. While the mathematical operations over two fuzzy sets A and B can be various such as union, intersection, equality, complement, dilation, and more, union and intersection operations are used for the fuzzy sets pressure drop $\mu(p\Delta)$ and vane angle $\mu(\beta_v)$ [20]. It is then possible to obtain a total number of ten rules, which can be found in Table 3.

Table 3. Obtained rules.

Rule	Inputs			Output
	β_v	Operator	Δp	d_{pc}
1	shallow	∩	low	huge
2	inclined	∩	low	medium
3	steep	∩	low	small
4	inclined	∩	moderate	huge
5	steep	∩	moderate	tiny
6	very steep	∩	moderate	tiny
7	steep	∩	high	small
8	very steep	∩	high	tiny
9	steep	∪	very high	tiny
10	very steep	∪	very high	tiny

2.3.3. Defuzzification

The fuzzy rules that form the boundaries of the fuzzy system (Table 3) usually have to be converted into a crisp output [20]. To transform the fuzzy results into crisp results, a defuzzification process is performed. The membership functions of the consequent fuzzy set $\mu(d_{pc})$ are displayed in Figure 8. Different methods of defuzzification are practiced, such as the center of gravity (COG), the center of sum (COS), the area center method (BOA), the weighted average method (WA), and the maximum methods (FOM, LOM, MOM). Each method leads to slightly different fuzzy results and is introduced in the following.

For the COS method, the center of the area under the membership functions of the fuzzy sets is recognized and weighted according to the size of the area. In the case of the COG method, all areas of the two fuzzy sets are handled separately, and the COG is calculated for each area. Further, the total COG of the unified or intersected area is calculated and weighted accordingly. The BOA method generates a value within the unified or intersected area where the size of the areas left and right to the value are equal in size. For the WA method, only symmetric membership functions are considered. The

maximum membership value weights the center of each function, and all values are added and divided by the sum of the maxima to solve for the center of the whole fuzzy set. For FOM, the minimum (first) value of the domain x with a maximum membership value $\mu(x)$ is examined. In contrast, for LOM, the domain's maximum (last) value is considered with the maximum membership value. MOM considers the mean value from maximum and minimum domain value x [22]. The fuzzy sets describing the particle size of particle cut diameter d_{pc} are namely $\mu_t(d_{pc})$, $\mu_s(d_{pc})$, $\mu_m(d_{pc})$ and $\mu_h(d_{pc})$ (cp. Table 2). In the case of the defuzzification of the membership functions of the consequent fuzzy set in the universe W

$$\mu(d_{pc}) = \mu_t(d_{pc}) + \mu_s(d_{pc}) + \mu_m(d_{pc}) + \mu_h(d_{pc}) = 1 \quad d_{pc} \in W \tag{14}$$

the defuzzification method BOA delivers the best results with the most minor error (cp. Table 4).

Table 4. Prediction error of different defuzzification methods using four membership functions.

Defuzzification Method	BOA	MOM	LOM	FOM	COG
Relative error ε in %	8.36	12.19	14.35	11.82	10.20
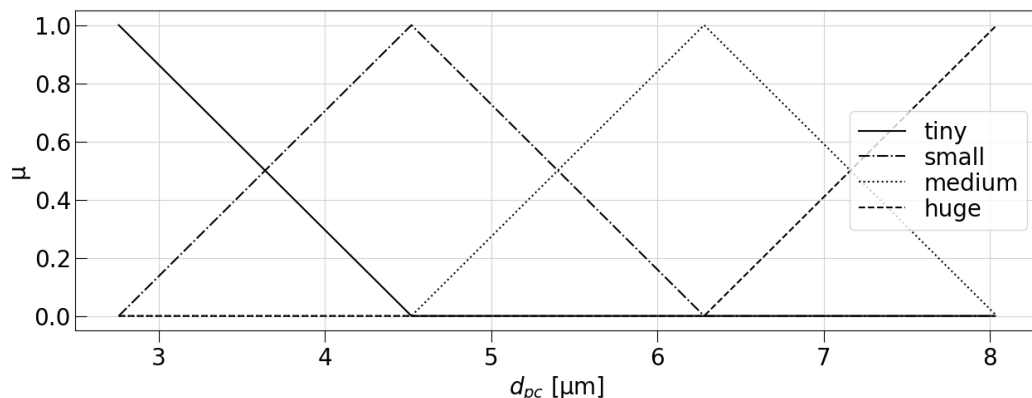
Figure 8. Membership functions of the particle cut diameter d_{pc}.

The definition of the membership function of the fuzzy set of the particle cut diameter can be found as

$$\mu_t(d_{pc}) = \begin{cases} 0 & for \quad d_{pc} \leq 2.76 \\ \frac{4.52 - d_{pc}}{2.76} & for \quad 2.76 \leq d_{pc} \leq 4.52 \\ 0 & for \quad 4.52 \leq d_{pc} \end{cases} \tag{15}$$

$$\mu_s(d_{pc}) = \begin{cases} 0 & for \quad d_{pc} \leq 2.76 \\ \frac{d_{pc} - 2.76}{2.76} & for \quad 2.76 \leq d_{pc} \leq 4.52 \\ \frac{6.28 - d_{pc}}{2.76} & for \quad 4.52 \leq d_{pc} \leq 6.28 \\ 0 & for \quad 6.28 \leq d_{pc} \end{cases} \tag{16}$$

$$\mu_m(d_{pc}) = \begin{cases} 0 & for \quad d_{pc} \leq 4.52 \\ \frac{d_{pc} - 4.52}{2.76} & for \quad 4.52 \leq d_{pc} \leq 6.28 \\ \frac{8.04 - d_{pc}}{2.76} & for \quad 6.28 \leq d_{pc} \leq 8.04 \\ 0 & for \quad 8.04 \leq d_{pc} \end{cases} \tag{17}$$

$$\mu_h(d_{pc}) = \begin{cases} 0 & for \quad d_{pc} \leq 6.28 \\ \frac{d_{pc} - 6.28}{2.76} & for \quad 6.28 \leq d_{pc} \leq 8.04 \\ 0 & for \quad 8.04 \leq d_{pc}. \end{cases} \tag{18}$$

3. Results and Discussion

3.1. Axial and Radial Velocities

As a base for the fuzzy logic prediction model for the particle cut diameter experimental data had to be acquired. The results of the experimental measurements are presented in the following. In Figure 9, the normalized axial velocity component U and the normalized radial velocity V can be seen for the specific Reynolds number $R_c = 13.9 \times 10^4$.
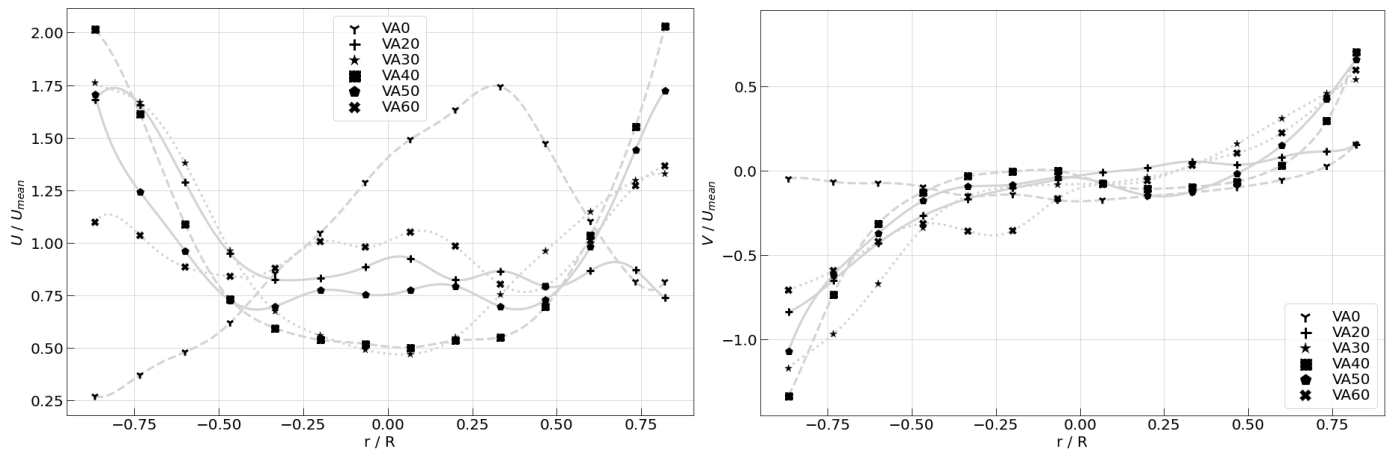
Figure 9. Normalized axial velocity U (**left**) and radial velocity V (**right**) at the entrance of the separation chamber for different vane angles β_v at Reynolds number $R_c = 13.9 \times 10^4$.

For the setup without the swirl inducer (VA0), the normalized axial velocity component U exhibits high velocity ratios near the tube center. In contrast, the axial velocity ratios near the wall are lower. With increasing vane angle β_v, the axial velocities decrease in the center and increase near the walls, resulting from the increased rotating motion around the tube axis. The normalized radial velocity shows a point symmetry around the tube axis due to the rotating motion of the swirled fluid (Figure 9). For VA0, the radial velocities are minimal. With increasing vane angle β_v, the curves of the radial velocities become steeper and reach a maximum for VA40. Further increasing the vane angle exhibit lower radial velocities at the near-wall area. These findings underline the inertia-based particle segregation capabilities of the system using the swirl inducers. The measured pressure drop over the uniflow cyclone setup ranged from $\Delta p = 22\,\text{Pa}$ to $546\,\text{Pa}$ in dependence on the swirl inducer vane angle β_v and the velocity setting (Figure 5), for which the Reynolds number Re_c varied between $R_c = 13.9 \times 10^4$ and $R_c = 25.2 \times 10^4$. The fractional efficiency curves for vane angles β_v from 0° to 59.7° of the swirl inducer with different Reynolds numbers R_c are calculated using the Equation (3). As suggested by Iozia [9], the data points of the fractional efficiency curve are approximated with a logistic curve

$$f(d_p) = \frac{1}{1 + e^{-\beta(d_p - d_{pc})}}. \tag{19}$$

While the midpoint of the logistic curve at a fractional efficiency of 50% represents the particle cut diameter d_{pc}, the slope parameter β describes the steepness of the midpoint.

3.2. Fractional Particle Separation Efficiency and Particle Cut Diameter

To determine the particle separation performance of the uniflow cyclone the fractional particle separation efficiencies for a particle diameter range d_p of 1 µm to 29 µm is measured with a particle spectrometer. The particle cut diameter d_{pc} is a measure for the overall separation efficiency within the given particle diameter range for the specific experimental setup. The fractional particle separation efficiencies for different swirl inducer vane angles β_v at a Reynolds number of $R_c = 13.9 \times 10^4$ are displayed in Figure 10.

Overall the particle cut diameter d_{pc} is calculated as in the range of 7.3 µm to 8 µm for vane angle $\beta_v = 0°$ (VA0), 5.8 µm to 7 µm for vane angle $\beta_v = 18.9°$ (VA20), 4.3 µm to 5.8 µm for vane angle $\beta_v = 29.7°$ (VA30), 3.5 µm to 4 µm for vane angle $\beta_v = 40.5°$ (VA40), 3.2 µm to 3.8 µm for vane angle $\beta_v = 48.8°$ (VA50) and 2.6 µm to 3 µm for vane angle $\beta_v = 59.7°$ VA60. All results on the particle cut diameter findings for Reynolds number $R_c = 13.9 \times 10^4$ to $R_c = 25.2 \times 10^4$ can be found in Table 5.
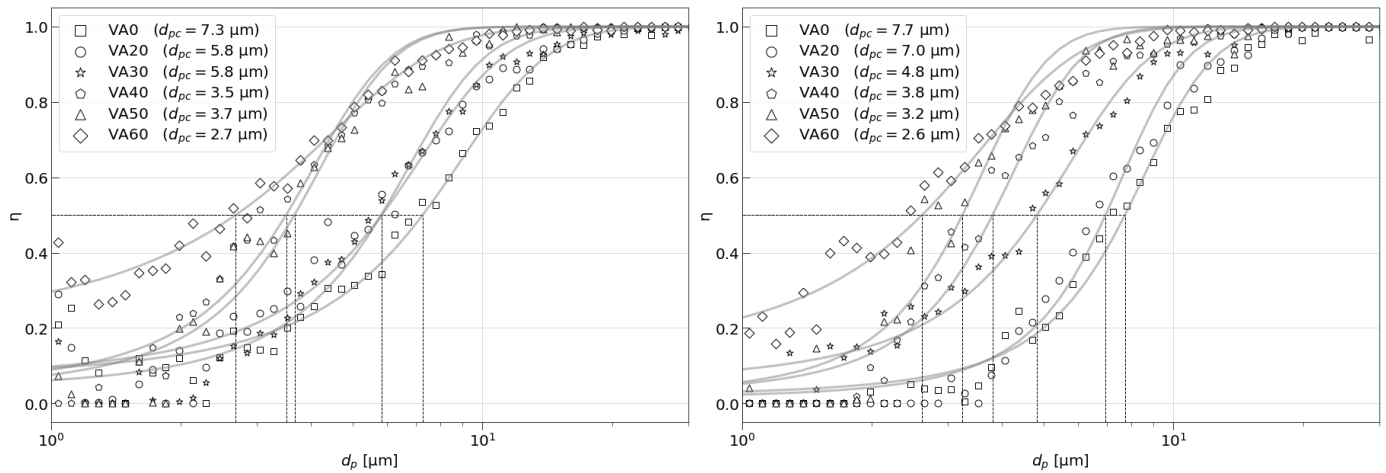
Figure 10. Fractional particle separation efficiencies η and particle cut diameter d_{pc} of the used swirl inducers for Reynolds number $R_c = 13.9 \times 10^4$ (**left**) and $R_c = 25.2 \times 10^4$ (**right**).

Table 5. Particle cut diameter d_{pc} in µm in dependence of the swirl inducer vane angle β_v and Reynolds number Re_c.

Re	VA0	VA20	VA30	VA40	VA50	VA60
13.9×10^4	7.3	5.8	5.8	3.5	3.7	2.7
20.0×10^4	8.0	6.6	4.3	4.0	3.8	3.0
25.2×10^4	7.7	7.0	4.8	3.8	3.2	2.6

The uniflow cyclone fractional particle separation efficiency curve exhibits lower fractional separation efficiencies for the fine dust for small particle diameters. In contrast, the efficiencies increase for larger particles as expected. The effect of the vane angle β_v of the swirl inducers is significant, as for larger vane angles β_v, the particle cut diameter d_{pc} is minimized (cp. Figure 10). Further, it is recognized that lower Reynolds numbers R_c, and therefore lower inlet velocity v_i, tend to have a positive but minor effect on the separation efficiency of the uniflow cyclone (Table 5). The lowest particle cut diameter d_{pc} of 2.6 µm is achieved with the swirl inducer vane angle of $\beta_v = 59.7°$, while for the lowest and highest tested Reynolds number Re_c, the particle cut diameter d_{pc} shows only a difference of 0.1 µm.

When comparing the particle cut diameter results for reverse-flow cyclones of past experimental research, the separation efficiency results of this study using a uniflow cyclone setup are promising, while reaching values close to the results of Stairmand and Dirgo & Leith [8].

While the particle density ρ_p ranges from 860 kg m^3 to 2650 kg m^3 in past studies [8,10], flow rates $\dot{v}$ from 15.0 L s^{-1} to 231.8 L s^{-1} were applied on cyclones with diameters d_c from 41 mm to 305 mm [8]. The achieved particle cut diameter d_{pc} ranges from 1.38 µm [8] to 5 µm [10]. This means that the achieved particle cut diameter d_{pc} in this study is comparable with the performance of past reverse-flow cyclone setups. Dirgo [8] and Iozia [9] used the mineral oil (Arcoprime 200) for their cyclone efficiency studies. Their achieved particle cut diameter d_{pc} was slightly larger than Stairmands results, but with higher pressure losses for similar cyclone diameters d_c. Beekmans [17], Klujszo [10], and Faulkner [19], on the other hand, used solid aerosol particles for their experiments. Klujszo [10] conducted

experiments with a uniflow cyclone system. However, for a particle diameter range d_p of 4 μm to 100 μm with a particle density ρ_p of 2650 kg m^3, the achieved particle cut diameter $d_{pc} = 5$ μm is the largest value in the considered research and the results of this study are out-performing the particle cut diameter d_{pc} achieved by Klujszo [10]. Previous experimental cyclone research has found various correlations with test parameters and the particle cut diameter d_{pc}. Consolidating the theories of Leith-Licht [23] and Barth [24], it was found that an increase in the cyclone diameter generally leads to a decrease in the particle cut diameter. These findings were confirmed by Beekmans [17], who used larger cyclone diameters d_c between 76 mm to 152 mm instead. Faulkner [19], on the other hand, achieved almost equal separation efficiencies η, while examining inlet velocities v_i from 10 m s^{-1} to 20 m s^{-1} (Table 6). The experimental data of Iozia [9] agreed very much with the findings of his predecessors. The discussed correlations and some of the empirical findings were partly numerically verified with computational fluid dynamic (CFD) by Gimbun [25], who analyzed the relationship between cyclone diameter d_c, fluid temperature T_{amb}, particle density ρ_p, and the separation efficiency η. An increase of each of these parameters was found to increase the separation efficiency η.

3.3. Performance of the Model

Since empirical models extracted from reverse-flow cyclone experiments only estimate the particle cut diameter for uniflow cyclones to a certain extent, developing prediction models is crucial. A fuzzy model is designed to predict the particle cut diameter of a uniflow cyclone. Based on the experimental data, linguistic domains, and fuzzy sets are created. After the defuzzification process described in the previous section, a crisp format is derived from the fuzzy membership functions. The predicted values of the particle cut diameter d_{pc} are further named $d_{pc\,pred}$. The particle cut diameter from the logistic curve $d_{pc\,meas}$ (cp. Table 5) is compared with the predicted particle cut diameter $d_{pc\,pred}$ gained from the defuzzification of the fuzzy logic system, and the relative error ε is calculated as

$$\varepsilon = \frac{\sum \left| \frac{d_{pcpred,i} - d_{pcmeas,i}}{d_{pcmeas,i}} \right|}{n}. \tag{20}$$

The coefficient of determination R^2 is a statistical measure to describe the performance of a model, which defines how well the predicted data fit the measured data. The coefficient of determination R^2 is computed as

$$R^2 = 1 - \frac{\sum \left(d_{pcmeas} - d_{pcpred} \right)^2}{\sum \left(d_{pcmeas} - \frac{\sum d_{pcmeas}}{n} \right)^2}. \tag{21}$$

The mean squared error (MSE), is calculated as

$$MSE = \frac{1}{n} \sum \left(d_{pcpred,i} - d_{pcmeas,i} \right)^2, \tag{22}$$

represents the mean distance between the predicted $d_{pc\,pred}$ and the measured particle cut diameter $d_{pc\,meas}$. The prediction of the particle cut diameter $d_{pc\,pred}$ using the experimental data set, is conducted with two to five fuzzy membership functions. The predicted particle cut diameter $d_{pc\,pred}$ is displayed in Figure 11 as a function of the measured values.

Table 6. Experimental parameters and results from previous studies in comparison (* indicates Stairmand-type cyclones).

	Particle Parameter			Geometrical Parameter				Process Parameter				
Category Symbol Unit	Aerosol Type	Particle Density ρ_p kg m^3	Cyclone Type	Cyclone Dia. d_c m	Cyclone 0 l_c m	Outlet Dia. d_e m	Particle Range d_p µm	Feed Rate c_i g m^{-3}	Inlet Velocity v_i m s^{-1}	Flow Rate $\dot{v}$ L s^{-1}	Pressure Drop Δp kPa	Cut Dia. d_{pc} µm
Stairmand (cited in [8])	n.a.	2000	reverse-flow *	0.203	0.8	0.1	n.a.	10	15.2	62.6	n.a. (~0.785)	1.38
Beeckmans [17]	uranine	n.a	reverse-flow	0.15	0.6	0.075	0.6–4.7	n.a.	6.1	19.1	n.a.	4.7
Dirgo & Leith [8]	min. oil	860	reverse-flow *	0.305	1.2	0.15	1–7	0.05	25	231.8	2.21	1.8
Iozia & Leith [9]	min. oil	876	reverse-flow	0.25	1.0	0.075–0.175	1.4–7.4	n.a.	15.2	95.0	0.40	3.2
Faulkner [19]	starch	1500	reverse-flow	0.15	0.616	0.072	17.95	2	16.3	42.5	0.32–1.03	4.7–5
Klujszo [10]	Arizona test dust A4	2650	uniflow	0.15	0.11–0.06	0.051	4–100	<5	7.4	15.0	n.a.	5
This study	Arizona test dust A1	2650	uniflow	0.15	1.0	0.086	1-40	0.0162	49.4	236.0	0.546	2.6
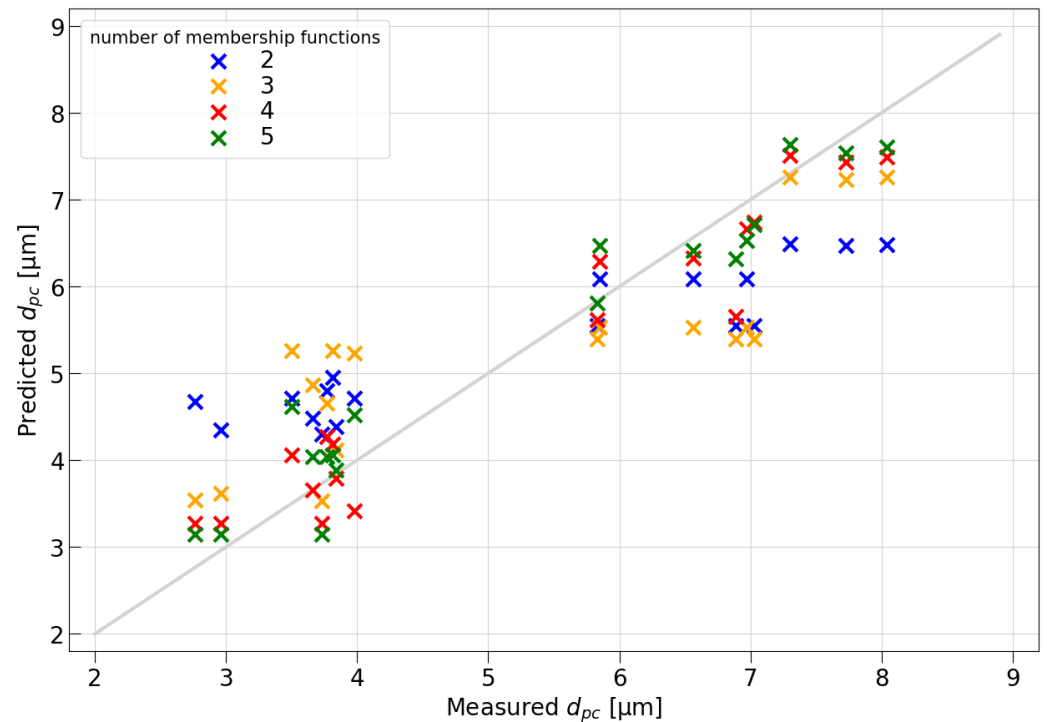
Figure 11. Comparison of the amount of membership functions and the respective prediction of the particle-cut diameter $d_{pc\,pred}$.

While with two and three membership functions, the particle cut diameter $d_{pc\,pred}$ does not match well with the particle cut diameter $d_{pc\,meas}$. The biggest effect in the reduction of the mean relative error ε is observed when increasing the membership functions from three to four. The mean relative error ε is reduced from $\varepsilon = 0.195$ to 0.084, while the coefficient of determination R^2 increases from 0.66 to 0.93. The computation of the particle cut diameter $d_{pc\,pred}$ using five membership functions in the fuzzy sets of the antecedent and consequent variables does not show a further decrease in the average relative error ε nor a valuable increase of the coefficient of determination R^2 (Table 7). A further increase of the amount of the fuzzy membership functions for the antecedent and consequent variables will increase the risk of over-fitting the logical model further. When the model focuses to much on reducing the MSE over-fitting is likely [26]. For test and train datasets this means that the relative error ε of the train dataset might be very low but in consequence the relative error ε of the a test dataset can be much higher. In the case of large data sets the use of a higher amount of linguistic terms and therefor of membership functions can be necessary. As the number of possible rules to define the fuzzy logic system are depending on the number of membership functions to the power of input variables, the computation time highly depends on the amount of rules used.

Table 7. Relative error ε, coefficient of determination R^2 and mean squared error (MSE) for different amount of membership functions

Membership Functions	Relative Error ε	Coefficient of Determination R^2	MSE
2	0.2189	0.6290	1.17
3	0.1947	0.6579	1.08
4	0.0836	0.9288	2.24×10^{-01}
5	0.0843	0.9344	2.06×10^{-01}

4. Conclusions

In this work, the performance of a uniflow cyclone system is examined. The particle size distribution is measured inside the cyclone outlet for three different Reynolds numbers R_c and six swirl inducer configurations with different vane angles β_v. The pressure drop Δp is measured for these 18 different combinations and the particle cut diameter d_{pc} is derived from a logistic curve that approximates the measured fractional particle separation efficiencies recorded for each particle size. The average fine dust injected into the cyclone system equals an air quality index (AQI) of 294. A similar AQI level can be found in Seoul, the Republic of Korea, and other densely populated cities worldwide on several days of the year. Therefore the particle density within the induced air is simulating a realistic fine dust pollution scenario. Compared with past experimental research, the data suggest that with a uniflow cyclone a particle cut diameter d_{pc} close to reverse-flow cyclone setups can be achieved for fine test dust with a particle diameter range d_p of 1 μm to 29 μm. Hence the experimental data underlines that uniflow cyclones perform on an almost equal level with reverse-flow cyclones while having the benefit of minor pressure losses and lower installation heights that usually do not exceed the cyclone diameter d_c. Consequently, uniflow cyclones can be installed in applications where the height is limited and easy access for maintenance is necessary.

The developed prediction model based on the fuzzy logic method provides excellent prediction results for the particle cut diameter d_{pc}, considering the experimental data and the clear structure of the model. Overall, the potential for uniflow cyclones is high, while their advantages compared to reverse-flow cyclone systems stand out. It is shown that with fuzzy logic models, a good prediction performance of the particle cut diameter d_{pc} requires careful consideration of the amount of used membership functions. Further highlighting the relationship between pressure drop Δp, swirl inducer vane angle β_v, and the cyclone efficiency, namely the particle cut diameter d_{pc}, this research provides the foundation for further cyclone research, especially in the case of uniflow cyclone systems.

5. Patents

During this research a resulting patent has been registered. The patent with the title "Method for removing particles by centrifugation based on rotating systems and centrifugal forces" has been registered at the Korean Intellectual Property Office under the patent no. 10-2490691.

Author Contributions: Conceptualization, V.K. and A.D.; methodology, V.K. and A.D.; software, V.K.; validation, V.K., G.L. and A.D.; formal analysis, V.K. and B.P.; investigation, V.K.; resources, V.K. and A.D.; writing—original draft preparation, V.K.; writing—review and editing, V.K., B.P. and G.L.; visualization, V.K. and B.P.; supervision, V.K., G.L. and A.D.; project administration, V.K. All authors have read and agreed to the published version of the manuscript.

Data Availability Statement: Any extra data needed can be provided by authors upon request.

Conflicts of Interest: The authors declare no conflict of interest.

Abbreviations

The following abbreviations are used in this manuscript:

BOA	bisector of area
COG	center of gravity
COS	center of sum
FDM	fuse-deposition modeling
FOM	first value of maximum
HEPA	high efficiency particulate air [filter]
LOM	last value of maximum
MOM	mean value of maximum

MSE   mean squared error
PSD   particle size distribution
VA   vane angle

References

1. Herald, K. Artificial Rain Test Failed to Ease Fine Dust Level. 2019. Available online: www.koreaherald.com/view.php?ud=2019 0227000638 (accessed on 28 September 2022).
2. Staudt, J.E. Control Technologies to Reduce Conventional and Hazardous Air Pollutants from Coal-Fired Power Plants. 2011. Available online: /www-f.nescaum.org/documents/coal-control-technology-nescaum-report-20110330.pdf/view (accessed on 3 October 2022).
3. Lapple, C.E. Gravity and Centrifugal Separation. *Am. Ind. Hyg. Assoc. Q.* **1950**, *11*, 40–48. [CrossRef]
4. Wadenpohl, C.; Löffler, F. Electrostatic agglomeration and centrifugal separation of diesel soot particles. *Chem. Eng. Process. Process Intensif.* **1994**, *33*, 371–377. [CrossRef]
5. *ISO 5167*; Measurement of Fluid Flow by Means of Pressure Differential Devices Inserted in Circular Cross-Section Conduits Running Full, 2nd ed. International Organisation for Standardization: Geneva, Switzerland, 2003.
6. *ISO 7708*; Air Quality—Particle Size Fraction Definitions for Health-Related Sampling, 1st ed. International Organisation for Standardization: Geneva, Switzerland, 1995.
7. Nel, A.; Xia, T. Toxic Potential of Materials at the Nanolevel. *Science* **2006**, *311*, 7. [CrossRef] [PubMed]
8. Dirgo, J.; Leith, D. Cyclone Collection Efficiency: Comparison of Experimental Results with Theoretical Predictions. *Aerosol Sci. Technol.* **1985**, *4*, 401–415. [CrossRef]
9. Iozia, D.L.; Leith, D. The Logistic Function and Cyclone Fractional Efficiency. *Aerosol Sci. Technol.* **1990**, *12*, 598–606. [CrossRef]
10. Klujszo, L.A.; Rafaelof, M.; Rajamani, R.K. Dust collection performance of a swirl air cleaner. *Powder Technol.* **1999**, *103*. [CrossRef]
11. Ngerntong, S.; Butdee, S. Surface roughness prediction with chip morphology using fuzzy logic on milling machine. *Mater. Today Proc.* **2020**, *26*, 2357–2362. [CrossRef]
12. Kasabov, N.K. *Foundations of Neural Networks, Fuzzy Systems, and Knowledge Engineering*; MIT Press: Cambridge, MA, USA, 1996.
13. Mahadevappa, J.; Groß, F.; Delgado, A. Fuzzy logic based process control strategy for effective sheeting of wheat dough in small and medium-sized enterprises. *J. Food Eng.* **2017**, *199*, 93–99. [CrossRef]
14. Janarthanan, R.; Balamurali, R.; Annapoorani, A.; Vimala, V. Prediction of rainfall using fuzzy logic. *Mater. Today Proc.* **2021**, *37*, 959–963. [CrossRef]
15. Greenworkstools 80V Cordless Brushless Blower GBL80320—Owner's Manual. 2014. Available online: https://cdn.shopify.com/s/files/1/0593/9537/5264/files/GBL80321_E.pdf?v=3671320346805040703 (accessed on 3 October 2022).
16. Litvinov, I.; Suslov, D.; Gorelikov, E.; Shtork, S. Swirl number and nozzle confinement effects in a flat-vane axial swirler. *Int. J. Heat Fluid Flow* **2021**, *91*, 108–812. [CrossRef]
17. Beeckmans, M. Analysis of the efficiency of reverse flow cyclones. *Can. J. Chem. Eng.* **1977**, *55*, 4. [CrossRef]
18. White, F. *Fluid Mechanics*; McGraw-Hill Series in Mechanical Engineering; McGraw Hill: New York, NY, USA, 2011.
19. Faulkner, W.B.; Shaw, B.W. Efficiency and pressure drop of cyclones across a range of inlet velocities. *Appl. Eng. Agric.* **2006**, *22*, 155–161. [CrossRef]
20. Debasis, S. Soft-Computing Applications. 2015. Available online: https://cse.iitkgp.ac.in/~dsamanta/courses/sca/index.html (accessed on 15 November 2022).
21. Dehzangi, O.; Zolghadri, M.J.; Taheri, S.; Fakhrahmad, S.M. Efficient Fuzzy Rule Generation: A New Approach Using Data Mining Principles and Rule Weighting. In Proceedings of the Fourth International Conference on Fuzzy Systems and Knowledge Discovery (FSKD 2007), Haikou, China, 24–27 August 2007; IEEE: Haikou, China, 2007; pp. 134–139. [CrossRef]
22. Dutu, L.C.; Mauris, G.; Bolon, P. A Fast and Accurate Rule-Base Generation Method for Mamdani Fuzzy Systems. *IEEE Trans. Fuzzy Syst.* **2018**, *26*, 715–733. [CrossRef]
23. Leith, D.; Licht, W. The Collection Efficiency of Cyclone Type Particle Collectors—A New Theoretical Approach. *Atmos. Environ. (1967)* **1972**, *68*, 196–206.
24. Barth, W. Berechnung und Auslegung von Zyklonabscheidern aufgrund neuerer Untersuchungen. *Brennst. Warme Kraft* **1956**, *8*, 1–9.
25. Gimbun, J.; Choong, T.S.Y.; Fakhru'l–Razi, A.; Chuah, T.G. Prediction of the Effect of Dimension, Particle Density, Temperature, and Inlet Velocity on Cyclone Collection Efficiency. *J. Teknol.* **2012**, *40*, 37–50. [CrossRef]
26. Jin, Y. On Generating FC Fuzzy Rule Systems from Data Using Evolution Strategies. *PART B* **1999**, *29*, 831–832.